Photovoltaic application of O-doped Wittichenite-Cu_3BiS_3: from microscopic properties to maximum efficiencies

C. Tablero

ABSTRACT

The electronic properties and the low environmental impact of Cu_3BiS_3 make this compound a promising material for low-cost thin film solar cell technology. From the first principles, the electronic properties of the isoelectronic substitution of S by O in Cu_3BiS_3 have been obtained using two different exchange–correlation potentials. This compound has an acceptor level below the conduction band, which modifies the opto-electronic properties with respect to the host semiconductor. In order to analyze a possible efficiency increment with respect to the host semiconductor, we have calculated the maximum efficiency of this photovoltaic absorber material. Copyright © 2012 John Wiley & Sons, Ltd.

KEYWORDS

ionization levels; electronic structure; semiconductors; impurities; photovoltaics

1. INTRODUCTION

The most extensively studied polycrystalline thin film solar cells are based on $Cu(In, Ga)(S, Se)_2$compounds. Although high-efficiency solar cells based on these materials have been produced, efforts are currently being made to develop new photovoltaic materials with suitable properties to be used in solar cells. The factors that should be considered in developing these new materials include the abundance of the precursor elements and the environmental impacts of their use. Cu_3BiS_3 is one of the most promising materials for low-cost thin film solar cell technology. As a photovoltaic absorber material for thin film heterojunction structures, Cu_3BiS_3 has a suitable electrical conductivity ($\sim 10^{-4}$ - 10^{-2} $\Omega^{-1}cm^{-1}$), optical absorption coefficient ($\sim 10^5$ cm^{-1} at 1.9 eV), and optical bandgap (1–1.6 eV) [1–3] for use as absorber layers in solar cells.

The compound Cu_3BiS_3 is a mineral, found in nature, with the Wittichenite structure (WS). Its structure (Figure 1) is orthorhombic ($a = 0.7723$ nm; $b = 1.0395$ nm; $c = 0.6716$ nm) [1–3]. This material has been grown using different procedures [1–7] and is a stable compound at room temperature. Some of the techniques used to deposit Cu_3BiS_3 thin films have been as follows: chemical bath deposition [2,4], reactive sputtering in one and two step processes [5], a rapid polyol process from single source precursors [6], and a simple ethanol–thermal process [7].

One of the goals of modern solid-state chemistry and physics is to analyze and fabricate new novel materials with suitable properties to be used as photovoltaic absorber materials and thus increase the efficiency of solar cells. The insertion of intermediate states within the bandgap of a semiconductor material provides additional paths for optical transitions creating the possibility for extremely high efficiency (>60%) [8].

Recently, II–VI compound semiconductors have attracted attention as a candidate for the realization of an appropriate intermediate band state using isoelectronic oxygen impurities. In particular, doping with oxygen has been shown to give rise to deep traps [9–12] at which carriers recombine radiatively [13,14].

Because Cu_3BiS_3 is one of the promising materials for solar cell applications and in order to further improve the conversion efficiency, it is important to investigate the

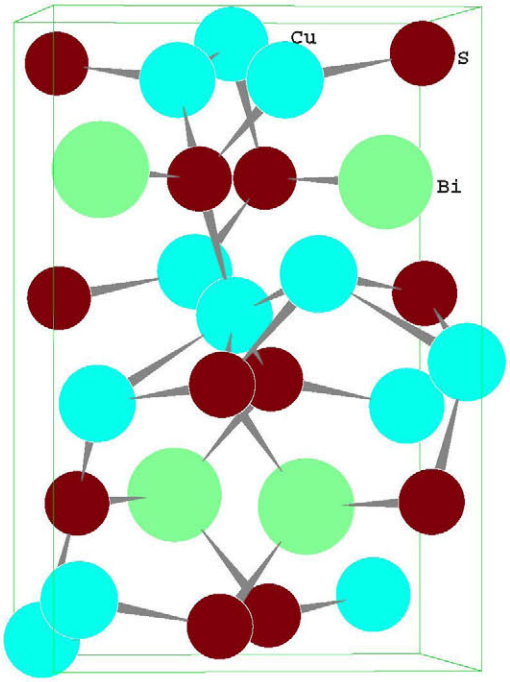

Figure 1. The crystal structure of the Cu_3BiS_3 compound in the WS.

effect of O doping in these compounds. The methodology applied in this analysis has been previously used to analyze other thin films [15].

2. METHODOLOGY

In this paper, we study the influence of substitutional incorporation of isoelectronic O impurities into S sites (O_s substitution) of Cu_3BiS_3 on its electronic and optical properties using the first principles within the density functional formalism [16,17]. For the exchange–correlation potential, we used the generalized gradient approximation (GGA) in the form of Perdew, Burke, and Ernzerhof [18] and the local density approximation (LDA) with the Perdew–Zunger parametrization to the Ceperley–Alder numerical data [19]. To use two exchange–correlation potentials, GGA and LDA, allows to evaluate the quality of the results.

The standard Troullier–Martins [20] pseudopotentials are adopted and expressed in the Kleinman–Bylander [21] factorized form. The valence wave functions are expanded in a numerically localized pseudoatomic orbital basis set [22].

It is known that the gaps obtained as differences of single-particle band structure energies (equivalent to using Koopman's theorem) are underestimated with LDA and GGA because of correlation problems. Nevertheless, if total defect formation energies [23,24] are used instead of single-particle energies, correlation problems and systematic errors are decreased [25]. Therefore, we use two different strategies in order to obtain the band edges and transition-energy levels at experimentally determined lattice constants: single-particle band structure calculations and total defect formation energies calculations. The former allows obtaining the single-particle band structure and density of states. The latter has a more direct relationship with the processes involved in the transitions. For example, the donor and acceptor energies for the O_s substitution correspond to the $O_S^0 \rightleftarrows O_S^{1+} + e$ and $O_S^0 + e \rightleftarrows O_S^{1-}$ transformations, respectively.

3. RESULTS AND DISCUSSION

In the WS (Figure 1) [1], the Cu is in nearly trigonal planar coordination with S (Cu-S distances between 0.225 and 0.235 nm and S-Cu-S angles between 110.8° and 131.8°). Bi is trigonally coordinated by S (Bi-S distances between 0.2569 and 0.2608 nm and S-Bi-S angles between 94.2° and 98.7°). S is tetrahedrally coordinated by three copper atoms and one bismuth atom. The energy–band diagram obtained using GGA for the Cu_3BiS_3 host and the O-doped Cu_3BiS_3(Cu_3BiS_3:O) around of the Γ point is shown in Figure 2. The results with LDA are similar, but

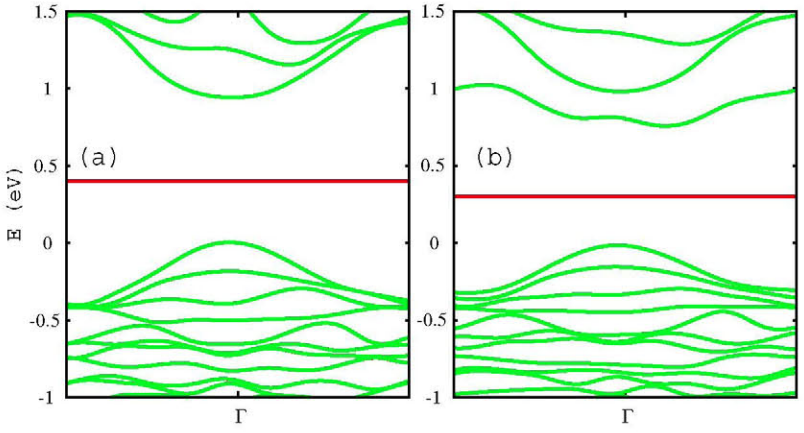

Figure 2. Energy–band diagram around the Γ point in the Brillouin zone with GGA for (a) the host Cu_3BiS_3 and (b) the O-doped Cu_3BiS_3. The VB edge has been chosen as the energy origin.

the gaps are slightly more underestimated. According to our results, the bandgap is 0.94 eV when GGA is used and 0.86 eV with LDA. Nevertheless, with defect formation energy calculations, the gaps are 1.27 eV (GGA) and 1.25 eV (LDA). These results compare well with the experimental results in the literature (between 1 and 1.6 eV) [1–3].

From Figure 2a, the Cu_3BiS_3 host has a direct bandgap, in agreement with previous experimental results [2,3]. By comparing the band structures (panels a and b), the substitution of S by O serves mainly to (i) push conduction band (CB) edge levels deeper into the gap and (ii) produce a slightly indirect gap. The Fermi energy (horizontal line in the figure) is between the valence band (VB) edge and the deeper CB level, indicating that this level has an acceptor character (without electrons).

From an analysis of the projected density of states on atoms (Figure 3a), we find that the CB edge in the host semiconductor is derived mainly from the combination of Bi orbitals with S and Cu orbitals (Figure 3a). When sulfur is substituted by oxygen, the O is tetrahedrally coordinated by three copper atoms and one bismuth atom. The O pushes the CB edge level, mainly constituted by the combination of Bi and O orbitals (Figure 3b), deeper into the gap.

Increasing the O concentration, the acceptor CB level will be converted in an acceptor band. With additional *n*-doping, the acceptor band can be partially populated with electrons. Then, the acceptor band can be transformed to a partially filled intermediate band (IB). The absorption of photons will be more efficient than in conventional solar cells because the absorption of low-energy photons causes transitions from the VB to the partially filled IB and from there to the CB. As well as this process of generating carriers, the usual process of generation through photon absorption promoting electrons from the VB to the CB also takes place.

Among the non-radiative recombination mechanisms, one of the most important related to the charge-transfer processes is the mechanism via multi-phonon emission (MPE) [26,27]. This mechanism is illustrated in Figure 4a, where the energy levels are represented with respect to a configuration coordinate Q. The MPE mechanism takes place when an impurity deep level is present. It occurs in two capture steps: an electron in the CB (e_{CB}) is first captured around Q_C in an impurity state A with energy e_A ($A + e_{CB} \rightarrow A^-$), then the electron recombines with a hole in the valence band around Q_V (hole capture $A^- + h_{VB} \rightarrow A$ or $A^- \rightarrow A + e_{VB}$, where h_{VB} (e_{VB}) represents a hole (electron) in the VB). The crossing point Q_C is the generalized coordinate where the electronic energy of the systems

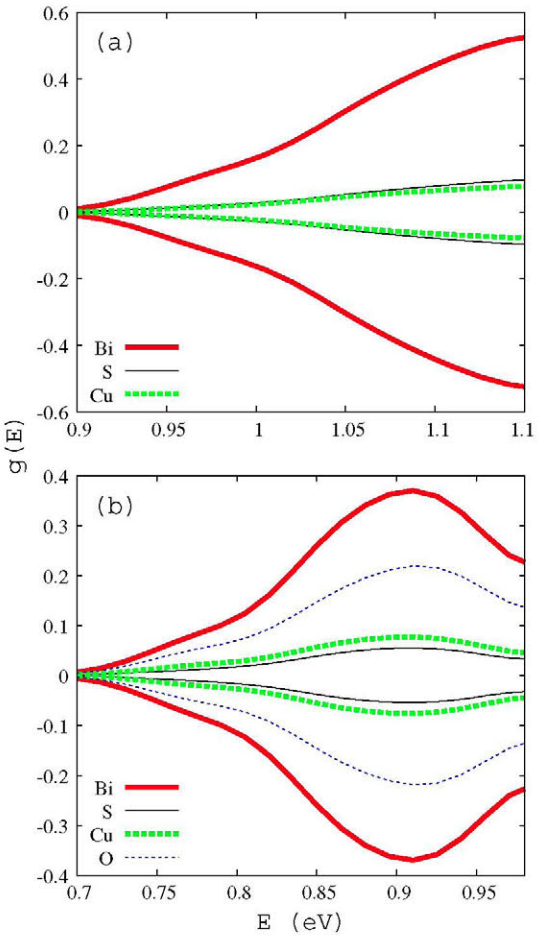

Figure 3. Projected density of states on the atoms for (a) the host Cu_3BiS_3 and (b) the O-doped Cu_3BiS_3. The VB edge has been chosen as the energy origin.

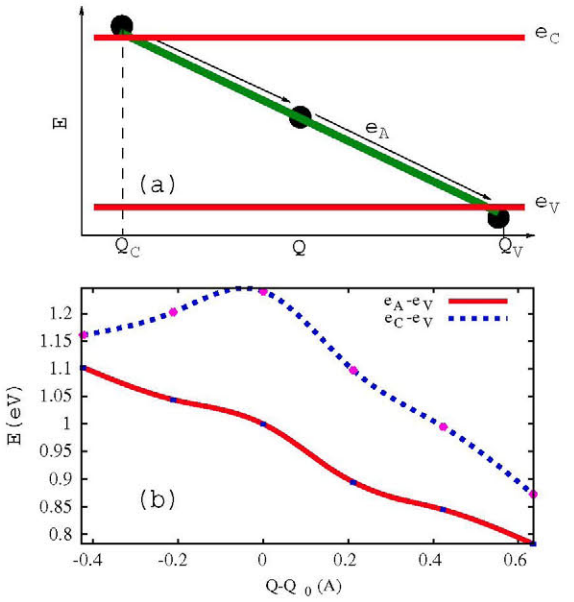

Figure 4. (a) Schematic representation of the non-radiative recombination as a function of the configuration coordinate Q. e_V, e_C, and e_A are the VB edge, CB edge, and acceptor CB–ionization energy, respectively. (b) CB edge and acceptor CB–ionization energy with respect to the VB edge energy as a function of $Q - Q_0$ for the O-doped Cu_3BiS_3.

$A + e_{CB}$ and A^- is equal. Similarly, the $A + e_{VB}$ and A^- energy curves cross in the generalized coordinate Q_V. After the transitions (captures), the large vibrational energy, which is initially localized at the impurity center, will propagate away from the center in the form of lattice phonons. Therefore, this mechanism is related with the inward and outward displacement of the nearest neighbors of the impurity atom, i.e., breathing modes [26,27].

The non-radiative recombination is inhibited when the energy levels involved in the non-radiative transition do not cross, or when the crossing point corresponds to very high energies with respect to the equilibrium configurations. From a microscopic point of view, there are two means of avoiding these crossings [27]: redistribution of the charge density because of the capture/emission of electrons/holes in the steps of the mechanism between all the impurities and redistribution of the charge density with the host semiconductor.

In order to study the MPE mechanism, we have considered the inward and outward displacement of the nearest neighbors of the O atom (Figure 4b). In this breathing mode, the distances between the O atoms and their nearest neighbors are scaled by an equal factor β with respect to the equilibrium positions Q_0: $Q = \beta Q_0$. In Figure 4b, the VB edge (e_V), CB edge (e_C), and acceptor CB–ionization energy (e_A) are obtained using defect formation energy calculations. From the figure, the NNR recombination is inhibited because the acceptor energy level does not cross with the CB and VB for a wide range of $Q - Q_0$. This is because of the redistribution of the charge density between all the impurities and with the host semiconductor. The latter is because of the acceptor band being mainly constituted by the O and Bi host orbitals (Figure 3b).

For *n*-doping to be effective, the donor impurity energy must be above or equal to the acceptor ionization energy of O-doped WS-Cu_3BiS_3 in the equilibrium position (Figure 4). Of course, with the increase of the O concentration, i.e., of the acceptor band, the energy of the donor energy impurity would be limited inferiorly by the acceptor band minimum. The PV device would also need to have a suitable carrier mobility. Nevertheless, in the IB solar cell model [8], the contacts are to the VB and CB, similar to that in conventional devices. The mobility in the VB and CB of the carriers for a material with an IB (impurity + host) is determined mainly by the electron–hole host mobility. High mobility in the IB is not essential because this band is not externally contacted [28].

Using defect formation energy calculations, the energy position of this deeper acceptor CB level (e_A) with respect to the CB edge ($e_C - e_A$) is 0.22 eV (GGA) and 0.24 eV (LDA). With these values, we have obtained the maximum efficiency for several sunlight concentrations (Figure 5). Calculations were carried out from 1 sun (1 Kw/m^2) to maximum solar concentration (46 050 suns) according to the model described in the study conducted by Luque and Martí [8], assuming that the sun is a blackbody at 6000 K and the cell operates at 300 K. For maximum solar concentration, the maximum efficiency obtained for Cu_3BiS_3:O with the results of GGA and LDA first-principles calculations is ~50%. This maximum is larger than the efficiency of a Cu_3BiS_3 single junction solar cell with equal solar concentration (~40%). The efficiency for Cu_3BiS_3:O is greater than that for Cu_3BiS_3 for all concentrations above 100 suns (Figure 5).

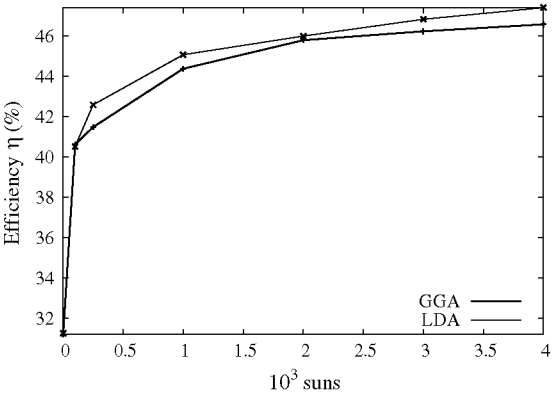

Figure 5. Efficiency η (%) versus sunlight concentration (10^3 suns) for GGA and LDA from defect formation energy calculations.

4. CONCLUSIONS

In conclusion, using first-principles density functional methods, we studied the electronic properties of the host and O-doped WS-Cu_3BiS_3. We have compared our results with the available experimental data and have analyzed the possible efficiency increment when the modified material is used as photovoltaic absorber material.

For the first-principles calculations, we used both LDA and GGA exchange–correlation potentials. In order to obtain gaps and impurity levels, we used both single-particle energies and total defect calculations. The results obtained compare well with experimental results in the literature. The acceptor energy levels in the gap for the O-doped WS-Cu_3BiS_3 form a band in the alloying limit. This band, below the CB edge, is the result of the Bi and O orbital combinations. Using the first-principles results, we have estimated the maximum efficiency of this photovoltaic absorber material. Above 100 suns, the efficiency of this compound is larger than the undoped host material with a single gap.

ACKNOWLEDGEMENTS

This work has been supported by the European Commission through the funding of the project IBPOWER (reference no.: Grant Agreement 211640) and by La Comunidad de Madrid through the funding of the project NUMANCIA-2 (reference no.: S-2009/ENE-1477).

REFERENCES

1. Kocman V, Nuffield EW. The crystal structure of wittichenite, Cu_3BiS_3. *Acta Crystallographica. Section B* 1973; **29**: 2528–2535.
2. Estrella V, Nair MTS, Nair PK. Semiconducting Cu_3BiS_3 thin films formed by the solid-state reaction of CuS and bismuth thin films. *Semiconductor Science and Technology* 2003; **18**: 190–194.
3. Mesa F, Gordillo G. Effect of preparation conditions on the properties of Cu3BiS3 thin films grown by a two step process. *Journal of Physics Conference Series* 2009; **167**: 012019.
4. Nair PK, Huang L, Nair MTS, H Hailin, Meyers EA, Zingaro RA. Formation of *p*-type Cu_3BiS_3 absorber thin films by annealing chemically deposited Bi_2S_3–CuS thin films. *Journal of Material Research* 1997: **12**: 651–656.
5. Gerein NJ, Haber JA. One-step synthesis and optical and electrical properties of thin film Cu_3BiS_3 for use as a solar absorber in photovoltaic devices. *Chemistry of Materials* 2006; **18**: 6289–6296.
6. Shen G, Chen D, Tang K, Qian Y. Synthesis of ternary sulfides Cu(Ag)-Bi-S coral-shaped crystals from single-source precursors. *Journal of Crystal Growth* 2003; **257**: 293–296.
7. Chen D, Shen G, Tang K, Liu X, Qian Y, Zhou G. The synthesis of Cu_3BiS_3 nanorods via a simple ethanol-thermal route. *Journal of Crystal Growth* 2003; **253**: 512–516.
8. Luque A, Martí A. Increasing the efficiency of ideal solar cells by photon ... transitions at intermediate levels. *Physical Review Letters* 1997; **78**: 5014–5017.
9. Tablero C. Acceptor and donor ionization energy levels in O-doped ZnTe. *Computational Materials Science* 2010; **49**: 368–371.
10. Tablero C. Analyses of the intermediate energy levels in ZnTe:O alloys. *Applied Physics Letters* 2010; **96**: 121104_1-121104_3.
11. Lee B, Wang L. Electronic structure of ZnTe:O and its usability for intermediate band solar cell. *Applied Physics Letters* 2010; **96**: 071903_1-071903_3.
12. Burki Y, Schwendimann P, Czaja W, Berger H. The temperature dependence of the photoluminescence and lifetime of ZnTe:O. *Journal of Physics: Condensed Matter* 1993; **5**: 9235–9252; Optical Gain in ZnTe: O at 2 K. *Europhysics Letters* 1990; **13**: 555–559.
13. Wang W, Lin AS, Phillips JD, Metzger WK. Generation and recombination rates at ZnTe:O intermediate band states. *Applied Physics Letters* 2009; **95**: 261107_1-261107_3.
14. Merz JL. Isoelectronic Oxygen Trap in ZnTe. *Physical Review* 1968; **176**: 961–968; Ge WK, Lam SB, Sou IK, Wang J, Wang Y, Li GH, Han HX, Wang ZP. Sulfur forming an isoelectronic center in zinc telluride thin films. *Physical Review B* 1997; **55**: 10035; Seong MJ, Alawadhi H, Miotkowski I, Ramdas AK, Miotkowska S. Oxygen isoelectronic impurity in ZnS_xTe_1. *Physical Review B* 1999; **60**: R16275; Yu YM, Nam S, Lee K-S, Dae Choi Y, Byungsung O. Photoluminescence characteristics of ZnTe epilayers. *Journal of Applied Physics* 2001; **90**: 807–812.
15. Tablero C, Fuertes Marrón D. Analysis of the electronic structure of modified $CuGaS_2$ with selected substitutional impurities: prospects for intermediate-band thin-film solar cells based on Cu-containing chalcopyrites. *Journal of Physical Chemistry C* 2010; **114**: 2756–2763; Tablero C. Ionization levels of doped sulfur and selenium chalcopyrites. *Journal of Applied Physics* 2009; **106**: 073718_1-073718_6; Tablero C. Electronic and magnetic properties of the Fe-doped $CuInS_2$. *Chemical Physics Letters* 2010; **499**: 75–78.
16. Kohn W, Sham LJ. Self-consistent equations including exchange and correlation effects. *Physical Review* 1965; **140**: A1133–A1138.
17. Soler JM, Artacho E, Gale JD, García A, Junquera J, Ordejon P, Sánchez-Portal D. The SIESTA method for *ab initio* order-*N* materials simulation. *Journal of Physics: Condensed Matter* 2002; **14**: 2745–2779.
18. Perdew JP, Zunger A. Self-interaction correction to density-functional approximations for many-electron systems. *Physical Review B* 1981; **23**: 5048–5079.
19. Ceperley DM, Alder BJ. Ground state of the electron gas by a stochastic method. *Physical Review Letters* 1980; **45**: 566–569.
20. Troullier N, Martins JL. Efficient pseudopotentials for plane-wave calculations. *Physical Review B* 1991; **43**: 1993–2003.
21. Kleinman L, Bylander DM. Efficacious form for model pseudopotentials. *Physical Review Letters* 1982; **48**: 1425–1428; Bylander DM, Kleinman L. 4*f* resonances with norm-conserving pseudopotentials. *Physical Review B* 1990; **41**: 907–912.
22. Sankey OF, Niklewski DJ. *Ab initio* multicenter tight-binding model for molecular-dynamics simulations and other applications in covalent systems. *Physical Review B* 1989; **40**: 3979–3995.
23. Van de Walle CG, Neugebauer J. First-principles calculations for defects and impurities: applications to III-nitrides. *Journal of Applied Physics* 2004; **95**: 3851–3879.
24. Northrup JE, Zhang SB. Dopant and defect energetics: Si in GaAs. *Physical Review B* 1993; **47**: 6791–6794.
25. Drabold DA, Estreicher S. Theory of Defects in Semiconductors. Springer: Berlin, Heidelberg, 2007.
26. Henry CH, Lang DV. Nonradiative capture and recombination by multiphonon emission in GaAs and GaP. *Physical Review B* 1977; **15**: 989–1016; *Physical*

Review Letters 1975; **35**: 1525; Boer KW. Survey of semiconductor physics. John Wiley & Sons Inc: New York, 2002.

27. Tablero C. Effects of the impurity–impurity and impurity–host interactions on the charge density and the related processes. *Physica B: Condensed Matter* 2009; **404**: 4023; Tablero C. Effects of the impurity–host interactions on the nonradiative processes in ZnS:Cr. *Journal of Applied Physics* 2010; **108**: 093114; Tablero C. Impurity–host interactions in Cr-substituted ZnSe. *Solid State Communications* 2007; **143**: 399–402.
28. Martí A, Cuadra L, Luque A. Quasi drift-diffusion model for the quantum dot intermediate band solar cell. *IEEE Transactions on Electron Devices* 2002; **49**: 1632–1639.